ELSEVIER

Journal of Luminescence 82 (1999) 177–186

JOURNAL OF LUMINESCENCE

Determination of the Judd–Ofelt parameters of the optical transitions of Sm^{3+} in lithiumborate tungstate glasses

H. Ahrens[a], M. Wollenhaupt[a], P. Fröbel[a], Jun Lin[a,1], K. Bärner[a,*], G.S. Sun[b], R. Braunstein[b]

[a]*IV. Physics Institute, University of Göttingen, Bunsenstr.11-13, D-37073 Göttingen, Germany*
[b]*University of California at Los Angeles, 405 Hilgard Ave., Los Angeles, CA 90024, USA*

Received 8 June 1998; received in revised form 28 April 1999; accepted 28 April 1999

Abstract

From the Sm^{3+}-related absorption peaks in different lithium–borate–tungstate glass matrices $((Li_2O)_{1-x}(B_2O_3)_x)_{100-y}(WO_3)_y$, oscillator strengths and with it charts of the Judd–Ofelt parameters for the whole glass-forming region in the borate rich corner of the system WO_3–Li_2O–B_2O_3 are given. These data are used to calculate the radiative fluorescence decay times, which are then compared with experimental fluorescence decay data. Deviations of up to a factor of 2 are attributed to the self-quenching effects in combination with different local environments for the Sm^{3+}-ions. © 1999 Elsevier Science B.V. All rights reserved.

Keywords: $((Li_2O)_{1-x}(B_2O_3)_x)_{100-y}(WO_3)_y$: Sm^{3+}; Optical absorption; Time resolved fluorescence; Fluorescence quenching

1. Introduction

Scattered data on the absorption and the fluorescence of Sm^{3+} in lithium–borate–tungstate glasses have been reported earlier [1–7].

However, so far no attempt has been made to systematically correlate the Sm^{3+}-related absorption with the integrated fluorescence peak intensities and/or decay times. This is, however, possible by making use of the Judd–Ofelt theory of rare earth–element optical transitions [8–13]. Judd and Ofelt have written the matrix elements of the transitions in different local environments as a weighted (Judd–Ofelt parameters Ω_i) sum of tabulated environment-independent matrix elements, i.e. those which can be classified by the J, L, S quantum numbers of the free ion states. As the absorption spectra usually contain a larger number of transitions, the three JO-parameters can, in principle, be obtained from three of the transitions. Then, the peak heights of the other transitions can serve as a test. However, as the height of any individual peak value can deviate by up to 10% from prediction, it is a better practice to carry out a least-squares fit over all available transitions. Once the JO-parametes are known, the strength and decay times of the fluorescent transitions can be calculated via the Einstein coefficients.

* Corresponding author. Tel.: + 49-551-39-4549; fax: + 49-551-39-4560.

E-mail address: baerner@ph4.physik.uni-goettingen.de (K. Bärner)

[1] Permanent address: Changchun Institute of Applied Chemistry, Chinese Academy of Sciences, Changchun 130022, China.

0022-2313/99/$ - see front matter © 1999 Elsevier Science B.V. All rights reserved.
PII: S0022-2313(99)00051-4

Table 1
(a) Colours of some of the measured lithium–borate–tungstate glasses. (b) Density ρ and refractive index n of some $[(LiO_2)_{1-x}(B_2O_3)_x]_{100-y}(WO_3)_y\,(Sm_2O_3)_z$ glasses

(a)

Structural colour centre $[(Li_2O)_{1-x}(B_2O_3)_x]_{100-y}(WO_3)_y$			Cu-related colour centre $(Li_2B_4O_7)_{99.9-z-y}(WO_3)_y(Sm_2O_3)_{0.1}(CuO)_z$		
x	y	colour	y	z	colour
0.25	8	Grey	0	0.1	Light blue
0.25	13	Blue	0	0.2	Light blue
0.25	20	Ceramic	0	0.3	Light blue
0.30	17	Transparent	0	0.5	Blue
0.30	19	Grey	0	1.0	Deep blue
0.30	20	Blue	10	0.3	Blue
0.33	20	Transparent	20	0.3	Blue
0.33	22	Grey	30	0.3	Greenish blue
0.33	25	Blue	40	0.3	Blueish green
0.80	3	Transparent	50	0.1	Light green
0.80	5	Grey	50	0.2	Light green
0.80	10	Blue	50	0.25	Green
0.80	13	Ceramic	50	0.3	Green
0.85	1	Transparent			
0.85	3	Blue			
0.90	2	Blue			
0.90	3	Ceramic			

(b)

x	y	z	ρ (g/cm^3)	n
0.10	0	0.3	1.98	1.476
0.15	0	0.3	2.05	1.498
0.15	0.5	0.3	2.29	1.530
0.20	0	0.3	2.13	1.519
0.20	5	0.3	2.38	1.535
0.20	8	0.3	2.39	1.537
0.20	10	0.3	2.59	1.558
0.25	0	0.3	2.12	1.546
0.25	0.5	0.3	2.23	1.550
0.25	10	0.3	2.67	1.562
0.25	16	0.3	2.92	1.596
0.30	0	0.3	2.35	1.552
0.30	5	0.3	2.44	1.554
0.30	10	0.3	2.77	1.572
0.30	15	0.3	2.92	1.594
0.30	20	0.3	3.19	1.623
0.30	25	0.3	3.32	1.634
2	0	1.0	2.26	1.556
2	10	1.0	2.39	1.567
2	20	1.0	2.65	1.572
2	30	1.0	2.88	1.598
2	40	1.0	3.13	1.604
2	50	1.0	3.42	1.633

In this contribution we have determined the JO-parameters from the Sm^{3+}-related absorption peaks in different lithium–borate–tungstate glass matrices, calculated the radiative fluorescence decay times τ_s and compared these with experimentally obtained decay times. From the deviations we have concluded various non-radiative fluorescence quenching mechanisms, in particular, two or more different environments which split the Sm^{3+} population.

2. Experimental

Powders of $Li_2B_4O_7$ (98%, Riedel deHaen (RdH), B_2O_3 (98%, RdH), WO_3 (99.5%, RdH), Sm_2O_3 (99.99%,Ventron), were mixed in the stoichiometric proportions, with a total weight of 4 g. The substances were thoroughly mixed, filled into an alumina crucible and subjected to a heat treatment: reaction temperature $T_r = 900°C$, reaction time $t_r = 10$ min (pure glasses): $T_r = 1000°C$, $t_r = 1$ h (Sm-doped glasses), in air. For annealing purposes, the melt was cast into a preheated (300°C) rectangular or flat aluminum vessel and retained there for 3 h. For the optical measurements two sample faces were polished, decreasing the grain size as follows: 180/240/360/600/1000: then a diamond paste polish was added: 5 μm, 3 μm. Table 1a and b show colour, refractive index and density, while Fig. 1 shows the glass forming region and the refractive index distribution in Li_2O–B_2O_3–WO_3 triangular concentration diagrams.

A double beam absorption spectrometer as described elsewhere [7] has been used to measure the Sm-related absorption. The spectrometer was modified to give optimal signal–to–noise conditions in the spectral range of the Sm^{3+} absorption, 0.4–1.4 eV. The source was a continuous spectrum tungsten-lamp (Osram). The obtained resolution at 488 nm was 2.5 nm. The inset of Fig. 2 shows largely structureless glass background absorption for various Li-contents in the region 0.4 –1.4 eV. The inset of Fig. 3 shows the energy levels of Sm^{3+} schematically. Details like level splittings and oscillator strengths might be slightly different in the different glass matrices. The fluorescence spectrometer used has also been described earlier [2], the excitation and collected fluorescent beam directions being at right angles. For the excitation we used the strong 488 nm line of a Lexel 75-1, 200 mW argon laser and sometimes a 750 W Xenon lamp (Beckmann) for comparison. The resolution of the fluorescence set-up was 0.03 nm [4].

The time-resolved fluorescence is measured as follows: the output of the argon laser (Lexel 75-1)

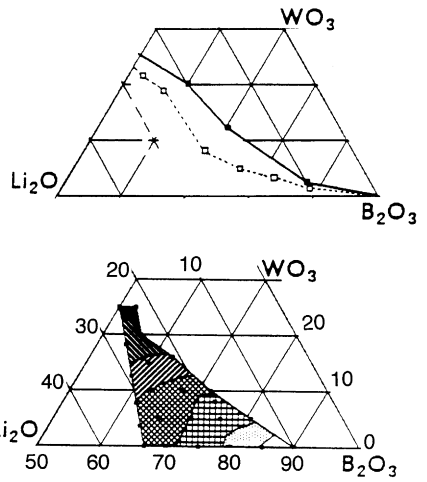

Fig. 1. Upper triangle: glass forming region of the borate–tungstate glasses: dashed line boundary for the appearance of bluish samples. Lower triangle: density; increasing darkness: 2, 2.25, 2.5, 2.75, 3, 3.25 (g/cm^3).

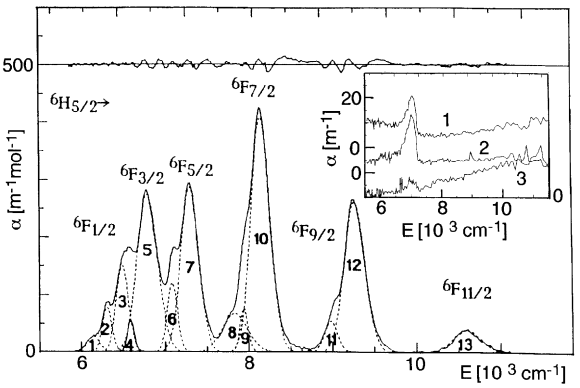

Fig. 2. Molar absorption of $(Li_2B_4O_7)_{99}(Sm_2O_3)_1$ versus quantum energy E. 1-13: resolved peaks, assigned to $^6H_{5/2} \rightarrow {}^6F_{n/2}$ transitions; line on top: deviation of fit from experiment; inset: absorption coefficient of $(Li_2O)_x(B_2O_3)_{100-x}$ glasses; from top to bottom: $x = 10, 15, 20$.

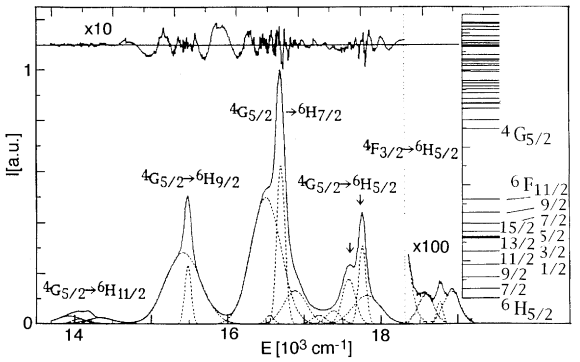

Fig. 3. Fluorescence intensity versus quantum energy $I(E)$ of $((Li_2O)_{0.30}(B_2O_3)_{0.70})_{99.9}(Sm_2O_3)_{0.1}$; peaks assigned to $^4G_{5/2}$, $^4F_{3/2}\rightarrow{}^6H_{n/2}$ transitions line on top: deviation of fit from experiment; inset: level scheme of Sm^{+3}.

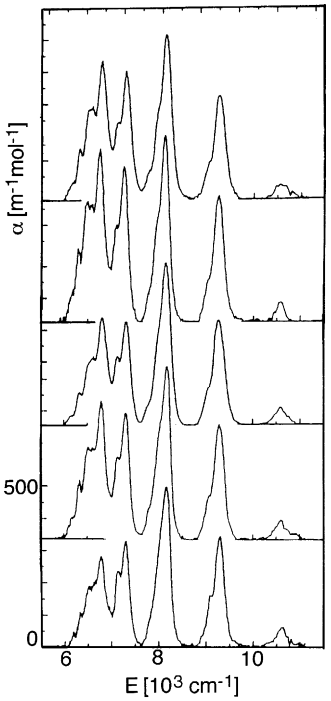

Fig. 4. Molar absorption versus quantum energy $\alpha(E)$ for different borate–tungstate glasses; from top to bottom: $(Li_2B_4O_7)_{100-x-1}(WO_3)_x(Sm_2O_3)_1$ $(x = 20, 40)$ $((Li_2O)_x \times (B_2O_3)_{1-x})_{100-y-0.3}(WO_3)_y(Sm_2O_3)_{0.3}$ $(x = 0.20,\ y = 0)$; $(x = 0.20,\ y = 10)$; $(x = 0.10,\ y = 0)$.

was focused on a fast rotating chopper blade, whose slit yielded a 50 μs light pulse with a repetition rate of 20 ms. The laser beam was then focused on the sample, the fluorescence light collected at a right angle and detected via a photomultiplier (Valvo XP1017). A low pass filter (Schott OG2) and slits were used to suppress scattered laser light and to accomodate the fluorescence light intensity. The signal was triggered by a partial reflection of the laser beam at a glass plate and appeared at a storage oscilloscope screen (Nicolet 1090A). Data processing followed using a DEC work station [14]. With laser excitation, we might have a partially selective excitation whose decay does not fully represent the decay of the total ion distribution. However, the apparatus was tested on a sample of $(Na_2B_4O_7)_{99.7}(Sm_2O_3)_{0.3}$: a lifetime of 2.4 ± 0.2 ms was obtained in accordance with the literature [15], suggesting that our decay curves are close. As we used a chopper blade to cut off the excitation light, we could measure using the xenon lamp. However, the deviations obtained in the structure and magnitude of the fluorescence decay stayed well within the error margins.

3. Results

3.1. Absorption spectra

Fig. 2 shows a typical absorption spectrum, whose peaks can be assigned to the J-L-S level diagram of Fig. 3. The absorption bands are tentatively decomposed into Gaussian peaks, whose number does not exceed the potentially split energy level pairs. Fig. 4 shows molar absorption spectra of Sm^{3+} in different borate–tungstate glass matrices. As expected, the spectra are only slightly modified by a variation of matrix. Note, that differences exist mainly in the peak heights while the peak positions are practically unchanged. Given the overlapping of the nearest-neighbour (N) electronic states with the 4f-states of Sm^{3+} and the point symmetry, the oscillator strengths and the splittings can in principle be calculated. Because of covalent bonding, the N- environment is supposed to be conserved to first order when changing the average matrix. Thus, the observed differences in the spectra are probably related to small variations in bond angle and length of the N-environment and to the next-nearest-neighbour (NN) occupancy.

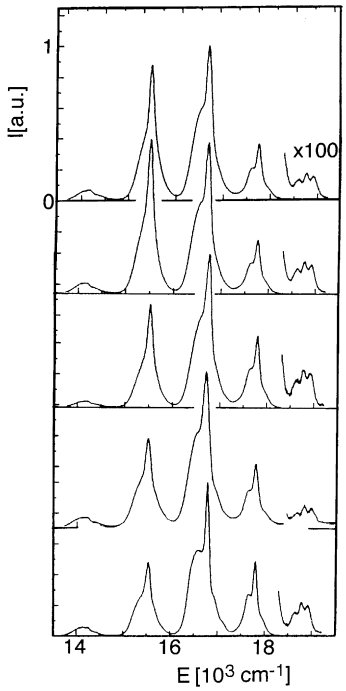

Fig. 5. Fluorescence intensity versus quantum energy $I(E)$ for different $((Li_2O)_x(B_2O_3)_{1-x})_{100-y-0.1}(WO_3)_y(Sm_2O_3)_{0.1}$ glasses; from top to bottom: ($x = 0.20$, $y = 0$); ($x = 0.20$, $y = 10$); ($x = 0.20$, $y = 10$): ($x = 0.10$, $y = 0$).

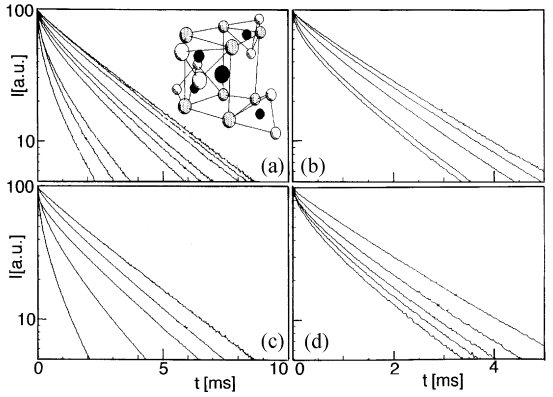

Fig. 6. Fluorescence decay curves $I(t)$ of some lithium-borate-tungstate glasses (a) $(Li_2B_4O_7)_{100-x}$ $(Sm_2O_3)_x$ (from top to bottom $x = 0.075, 0.15, 0.30, 0.75, 1, 1.2, 1.6, 2.1, 2.9$); (b) $(Li_2B_4O_7)_{50-x}(WO_3)_{49}(Sm_2O_3)_x$ (from top to bottom : $x = 0.1, 0.2, 0.6, 1, 1.1$); (c) $(Li_2B_4O_7)_{99.9-x}(Sm_2O_3)_{0.1}(CuO)_x$ (from top to bottom : $x = 0, 0.2, 0.3, 0.5, 1$); (d) $(Li_2B_4O_7)_{49.9-x}(WO_3)_{50}(Sm_2O_3)_{0.1}(CuO)_x$ (from top to bottom : $x = 0, 0.1, 0.2, 0.25, 0.3$).

3.2. Fluorescence spectra

Fig. 3 shows a typical fluorescence spectrum. Again the peaks can be related to the level scheme and the spectrum is tentatively decomposed into Gaussian peaks. The relative peak heights can change by a factor of two for different borate–tungstate glass matrices, while the peak positions remain practically unchanged (Fig. 5, $\Delta E < 40\,cm^{-1}$). Apparently, not only the hypersensitive fluorescence transitions but also all the fluorescence peaks are more sensitive to the changes in the NN-environment as the absorption peaks.

3.3. Fluorescence decay

The fluorescence and absorption spectra should be correlated through the JO-parameters. However, if the fluorescence spectra involve transition path's and non-radiative processes which are related to two or more different Sm^{3+}-sites, as indicated by the broadness of the spectra, the correlation might be poor. An alternative would be to correlate the absorption spectra with the fluorescence decay times. Here, one might be able to discriminate the populations by their respective lifetimes and thus correlate the calculated radiative decay time with a selected experimental lifetime. In particular, using the longest lifetime would probably select the population which suffers the least non-radiative energy transfer.

Fig. 6 shows the time-resolved fluorescence curves obtained for different Sm-contents. Because of cross-relaxation the lifetime generally decreases with increasing Sm-content. Slightly non-exponential decays can be ascribed to a random distribution of the absorbers. However, at larger Sm-contents a second lifetime is suggested: an initial drop-off precedes a later slower relaxation. Similar curves are obtained if one intentionally co-dopes with copper (Fig. 6c and d) which acts as an acceptor state. In this case, evidence for two different Sm^{3+} populations has been claimed [4].

4. Discussion

4.1. Stark splittings

4.1.1. Absorption lines

As the crystal electric field generally removes some of the degeneracies of the Sm^{3+} ionic states and since these overlap with the nearest-neighbour atomic states to some extent, J, L, S are not good quantum numbers anymore. However, it is customary to still classify the 4f states by their J - multiplicity. In particular, a very similar $^6H_{5/2} \rightarrow {}^6F_{n/2}$ spectrum has been measured for Sm^{3+} in a $POCl:SmCl_4$ solution, supporting both the choice of valence state (3 +) and the generally weak impact of the nearest neighbour environment on the 4f- states. This spectrum has also been used to check the assignments, which rely on line centre positions and relative peak heights as obtained from the literature [16,17]. In particular, all the $^6H_{5/2} \rightarrow {}^6F_{n/2}$ absorption lines appear to be threefold split, which is thought to arise from a threefold splitting of the $^6H_{5/2}$ ground state in the crystal field. Note, that if one does not have three Gaussians per main peak, one of the peaks is broadened, suggesting a convolution. The $^6F_{1/2}$ triplet is best resolved, when the Stark splittings are 150 and 340 cm^{-1}, in accordance with the literature [5]. The $^6F_{n/2}$ levels could be split, too [18].

4.1.2. Fluorescence lines

For the fluorescence spectra the deconvolution into Gaussian lines is less convincing as it was the case for the absorption spectra. The very small Gaussians are probably artefacts arising from the strong overlap of various transitions which could not be properly resolved. However, the threefold splitting of the $^6H_{5/2}$ ground state can readily be found again in the two transitions which involve this state as the lower level. The initial states $^4G_{5/2}$ and $^4F_{3/2}$ could be split into 3 and 2 levels, too. In principle, also the $^6H_{n/2}$ levels could split: into 3, 4, 5 and 6 Kramers doublets for $n = 5, 7, 9$ and 11 [18,19].

4.2. Determination of the Judd–Ofelt parameters

In defining the experimental oscillator strengths, P^i, from the observed absorption lines (i) we follow Ref. [17]:

$$P^i_{exp} = (mc^2/\pi Ne^2)\int_i \alpha(E)\mathrm{d}E \quad (1)$$

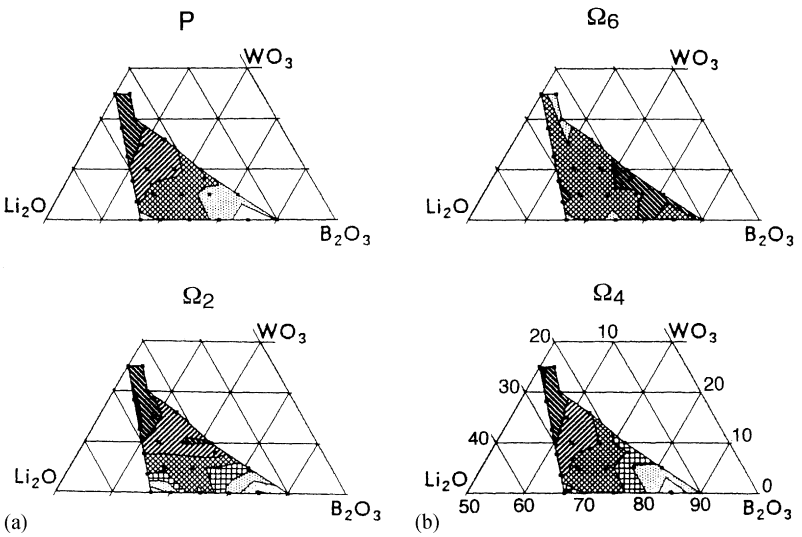

Fig. 7. (a and b) Distribution of the oscillator strength of the $^6H_{5/2} \rightarrow {}^6F_{5/2}$ transition in units of 10^6 and of the Judd–Ofelt parameters Ω_2, Ω_4, Ω_6 in units of 10^{-20} cm^2 in the glass forming region of the borate-tungstate glasses. (a) P : increasing darkness : 1.75, 2, 2.25, 2.5; Ω_2 : 3, 3.5, 4, 4.5, 5, 5.5, 6; (b) Ω_4 : 3.25, 3.5, 3.75, 4, 4.25, 4.5, 4.75; Ω_6 : 2.2, 2.4, 2.6.

where, e, m are the electronic charge and mass, N the Avogadro's number, α the molar absorption constant, c the light velocity.

Fig. 7 shows the compositional chart $P \times 10^6$ for the $^6H_{5/2} \rightarrow {}^6F_{5/2}$ transition as an example. All the $^6H_{5/2} \rightarrow {}^6F_{n/2}$, $n = 1$–9, transitions have comparable oscillator strengths, while the one into $^6F_{11/2}$ is an order of magnitude lower.

The oscillator strengths according to the Judd–Ofelt theory [8.9] are:

$$P^J = (\chi 8\pi^2 mcE)/(3h(2J+1) \times \sum_{\lambda=2,4,6} \Omega_\lambda \langle JLS|D^\lambda|J'L'S'\rangle_\lambda^2 \quad (2)$$

where J, L, S are the angular momentum quantum numbers, $\chi = (n+2)^2/9n$ is the Lorentz correction of refractive index n, h the Planck's constant and D^λ the electrical dipole operator.

As P^i_{exp} and the quantities in the prefactor are known and the bracketed matrix elements tabulated, one can calculate the three JO-parameters Ω_2, Ω_4 and Ω_6. Fig. 7 shows the concentration charts of the JO-parameters obtained this way.

The JO-parameters are close to literature [30] and get smaller in increasing order, i.e. the maxima are almost inversely related $\Omega_2/\Omega_4/\Omega_6 = 6/4/2$. Also, their charts are different; while the Ω_6-chart, holding the smallest values, is rather unsystematic, suggesting that systematic errors might already be introduced, both the Ω_2- and Ω_4-charts seem to reflect the oscillator strengths, suggesting some common cause. In particular, for Ω_2 and Ω_4, the values tend to increase towards the Li_2O–WO_3 baseline. It is thought, that Ω_2, Ω_4 tend to increase when oxygen moves towards the Sm^{3+}- ion. Ω_2 is additionally increased, if the linear field term at the Sm-site is enhanced; this could also be done by getting the oxygen closer to Sm^{3+}. However, the structural units of the glass matrix are the boron triangles, the boron and tungsten tetrahedra and the tungsten octahedra. The O–O distance in a boron-tetrahedron is 0.24 nm [20], 0.32 nm in a tungsten-tetrahedron [21] and 0.26 in a tungsten-octahedron [22]. Thus the Sm–O distance is not expected to be reduced with increasing WO_3-content; at best, angular distortions increase.

Ω_2 is also increased if the matrix tends to become dielectrically more inhomogeneous [13]. This happens with increasing the WO_3-content as the compound WO_3 is ferroelectric and as the WO_3-units tend to form clusters. The dielectric inhomogeneity is probably the most important factor, as it is consistent with the fact that Ω_2 increases fastest towards Li_2O–WO_3 and that the refractive index increases the same way (Fig. 1).

4.3. Radiative relaxation times

The Einstein coefficients for spontaneous emission can now be written as [23]:

$$A^i = (\chi' 64\pi^4 e^2 E^3)/(3h(2J+1) \times \sum_{\lambda=2,4,6} \Omega_\lambda \langle JLS|D^\lambda|J'L'S'\rangle_\lambda^2, \quad (3)$$

where $\chi' = \chi n^2$ is the Lorentz correction.

As the coefficients for spontaneous emission equal the reciprocal radiative relaxation time, $A^i = \tau_s^{-1}$ and as the relative amplitudes of the fluorescence transitions are given by $a_i = A_i/\Sigma A_j$, one can predict the fluorescence spectra as well as the fluorescence decay times.

Here, we choose to correlate the absorption matrix elements with the relaxation times of the fluorescence decay. Part of eventual inconsistencies could be simply related to the error propagation, to the selective excitation or to the shortcomings of the theory. However, the influence of competing relaxation channels due to the multiphonon processes and the interference of the weaker magnetic dipole or electric quadrupole transitions should be numerically small here [13,24,25]. The largest error source probably originates from the quite large Stark splittings: the JO-theory averages over the individual Stark levels of a JLS state. However, in reality these levels are not equally populated.

The non-exponential decay curves which are observed experimentally (Fig. 6) pose another problem; they can, however, be simulated by two different Sm^{+3} populations which have strongly different JO-parameters and close ($> 10\%$) relaxation times or, alternatively, they might have close JO-parameters and strongly unequal lifetimes. In the actual curve fit, we distinguish three empirical

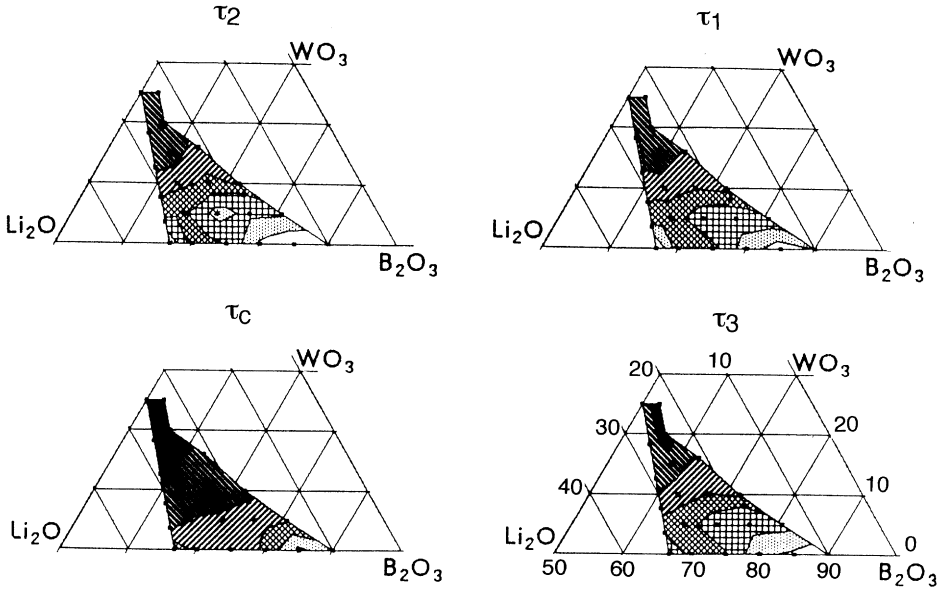

Fig. 8. Distribution of the calculated τ_c and the empirical relaxation times τ_i in ms in the glass forming region of the lithium–borate–tungstate glasses. τ_c : increasing darkness : 5, 4.5, 4, 3.5, 3, τ_1 : 2.75, 2.5, 2.25, 2, 1.75, 1.5, τ_2 : 3, 2.75, 2.5, 2.25, 2, 1.75, τ_3 : 3.25, 3, 2.75, 2.5, 2.25, 2.

Table 2
Fluorescence decay relaxation times and Judd–Ofelt parameters for two glass series as specified

$(LiO_2)_{67(1-2.5z)}(B_2O_3)_{33(1+2z)}(WO_3)_{100z}$

100 z	τ_3(exp) (ms)	τ(calc) (ms)	$\Omega_2(10^{-20})$cm^2	Ω_4	Ω_6
0	2.85 ± 0.05	4.25	3.1	3.8	2.3
5	2.75	3.5	4.5	4.25	2.6
10	2.4	3.25	5.0	4.4	2.4
15	2.15	3.1	6.0	4.6	2.5
20	2.1	2.75	6.5	4.65	2.5
25	2.0	2.2	5.8	4.75	2.6
[30]	—	—	0.91	4.13	2.7

$(LiO_2)_{70(1-2.7z)}(B_2O_3)_{30(1+3z)}(WO_3)_{100z}$

100 z	τ_3(exp) (ms)	τ(calc) (ms)	$\Omega_2(10^{-20})$cm^2	Ω_4	Ω_6
0	2.6	4.0	3.4	4.0	2.4
5	2.5	3.5	4.6	4.2	2.4
10	2.35	3.25	5.2	4.3	2.5
15	2.15	3.0	5.6	4.5	2.5
20	2.0	2.85	5.75	4.6	2.3
25	2.0	2.75	5.8	4.75	2.2

relaxation times: τ_1, τ_2, τ_3. Fig. 8 shows the chart of τ_s together with the charts of the τ_i. $\tau_s = \tau_c$ is closest to and its chart correlates best with the longest relaxation time τ_3 (see also Table 2).

4.3.1. Fluorescence quenching

The mechanisms of fluorescence quenching (FQ) are usually analysed through an investigation of the concentration dependence of the partner to whom the energy is transfered, i.e. Sm^{3+} in the case of cross-relaxation or a co-doped acceptor state concentration.

4.3.2. Cross-relaxation

The fluorescence per Sm-ion decreases with increasing Sm-content. This loss in the quantum yield is called selfquenching; it happens, for example, through cross-relaxation: an excited Sm-ion transfers energy by electric multipole interaction to a neighbouring Sm-ion in the ground state. Both ions then enter into an $^6F_{n/2}$ state, as these are

conveniently located in the middle of the $^4G_{5/2} - {}^6H_{5/2}$ level gap. In particular, the pairs ($^4G \rightarrow {}^6F$ and $^6H \rightarrow {}^6F$) : (5/2-9/2) and (5/2-9/2); (5/2-7/2) and (5/2-9/2); (5/2-5/2) and (5/2-11/2) are situated well. The coupling is primarily mediated by either dipole–dipole or dipole–quadrupole interactions [26,27].

In order to find out the coupling mechanism here, one may apply the Inokuti–Hiramaya formula [28] to the Sm-only fluorescence decay:

$$\Phi(t) = \exp(-t/\tau - \Gamma(1 - 3/s)(c/c_0)(t/\tau)^{3/s}), \qquad (4)$$

where τ is the donor lifetime without acceptors, c the acceptor concentration, $c_0 = 3/(4\pi R_0^3)$ critical concentration, R_0 the critical distance where the transfer rate equals the donor internal relaxation rate, Γ the gamma-function, $s = 6, 8$ and 10 for dipole–dipole, dipole–quadrupole, quadrupole–quadrupole interaction, respectively. The best fit for Sm^{3+} as an acceptor gives $s = 8$, i.e. a dipole-quadrupole interaction for both the borate and the borate–tungstate glasses. Deviations from Eq. (4) might be due to a (eventually split) site distribution. However, as Stark splittings can be resolved in some cases, the single-peak distribution width appears to be small. This might be due to a certain self adjustment of the Sm^{+3} environments in these glass matrices.

4.3.3. Energy transfer into other acceptor states

Copper (Cu^{2+}) is an acceptor state which is suspected to split the Sm^{+3} population, as the local quantum yield versus Cu-content could not be fitted to a single-Inokuti–Hirayama function [4,28,29]. Here too, the fluorescence decay curves are non-exponential and similar to the Sm^{3+} related decay curves. From the FQ of Cu^{2+} and the possible impurity content one can estimate an upper limit for the amount of fluorescence quenching from unintentionally introduced impurities. This contribution turned out to be negligible. Eq. (4), $s = 6$ gave the best fit, suggesting dipole–dipole interactions for Cu^{+2} - Sm^{+3} pairs, independent of the WO_3-content. This difference in multipole interaction again suggests that impurities play a minor role as compared to selfquenching of Sm^{+3} ($s = 8$).

From the relative increase in the initial slope of the fluorescence decay with increasing WO_3-content one may conclude, that the Sm^{3+} populations split deeper with increasing WO_3-content. For this the change in the type of NN-neighbours might be responsible, as the borate tetrahedrons (inset Fig. 6) of the matrix get increasingly replaced by W-tetrahedrons and W-octahedrons. Here again, a certain bond-adjustment of the Sm^{+3}, directed towards a symmetry increase [16] is necessary to create a two peak distribution.

5. Conclusions

Lithiumtungstateborate glasses harbor a variety of color- and fluorescence centres which can be used for modelling typical glass applications or as sensors for the investigation of the structure of amorphous matrices. In this contribution flourescence centre data points are set over the whole glass forming region, which provides a guideline for a future more detailed research.

Acknowledgements

The authors would like to thank the Deutsche Forschungsgemeinschaft for continuous support and G.H. Rao for useful comments. One of us is also indebted to the DAAD - K.C. Wong foundation.

References

[1] M.v. Dirke, S. Müller, K. Bärner, J. Non-Cryst. Solids 124 (1990) 265.
[2] S. Müller, P. Fröbel, K. Bärner, J. Non-Cryst. Solids 127 (1991) 323.
[3] R. Staske, P. Fröbel, M.v. Dirke, S. Müller, K. Bärner, Solid State Commun. 78 (1991) 647.
[4] R. Staske, P. Fröbel, K. Bärner, J. Lumin. 55 (1993) 115.
[5] J. Maaß, M. Wollenhaupt, H. Ahrens, P. Fröbel, K. Bärner, J. Lumin. 62 (1994) 95.
[6] M. Wollenhaupt, H. Ahrens, P. Fröbel, K. Bärner, E.A. Giessinger, R. Braunstein, J. Non-Cryst. Solids. 9312 (1995) XXX.
[7] P. Fröbel, K. Bärner, J. Non-Cryst. Solids 88 (1986) 329.
[8] B.R. Judd, Phys. Rev. 127 (1962) 750.

[9] G.S. Ofelt, J. Chem. Phys. 37 (1962) 511.
[10] B.R. Judd, J. Chem. Phys. 44 (1966) 839.
[11] B.R. Judd, J. Chem. Phys. 70 (1979) 4830.
[12] C.K. Jorgensen, Structure and Bonding, Vol. 22, Springer, Berlin 1975, p. 83ff.
[13] C.K. Jorgensen, B.R. Judd, Molecular Phys. 8 (1964) 281.
[14] H. Ahrens, Diplomarbeit, Göttingen 1994.
[15] J.C. Joshi, J. Joshi, R. Belwal, B.C. Joshi, N.C. Pandey, J. Phys. Chem. Solids. 39 (1978) 581.
[16] R. Reisfeld, J. Res. Nat. Bureau Standards A76 (1976) 613.
[17] W.T. Carnall, P.R. Fields, K. Rajnak, J. Chem. Phys. 49 (1968) 4424.
[18] N.C. Chang, J.B. Gruber, R.P. Leavitt, C.A. Morrison, J. Chem. Phys. 76 (1982) 3877.
[19] T.T. Basiev, M.A. Borik, Yu.K. Voronko, V.V. Osiko, V.S. Fedorov, Opt. Spectros. (USSR) 46 (1979) 510.
[20] Gmelin Handbuch der Anorg. Chemie, 8th Edition, Vol. 28, part 7, Springer, Berlin, p.58.
[21] I. Lindquist, Acta Chem. Scand. (1950) 1066.
[22] E. Salje, Acta Crystallor. A 31 (1975) 360.
[23] L. Boehm, R. Reisfeld, N. Spector, J. Solid State Chem. 28 (1979) 75.
[24] H.W. Moos, J. Lumin. 1/2 (1970) 106.
[25] W.T. Carnall, P.R. Field, K. Rajnak, J. Chem. Phys. 49 (1968) 4412.
[26] Z. Zhang, X. Jiang, Z. Li, P. Wu, S. Xu, J. Lumin. 40/41 (1988) 657.
[27] V.D. Rodriguez, I.R. Martin, J. Lumin. 54 (1992) 231.
[28] M. Inokuti, F. Hirayama, J. Chem. Phys. 43 (1965) 1978.
[29] T.C. Pant, B.C. Bhatt, D.D. Pant, J. Lumin. 10 (1975) 323.
[30] W.T. Carnall, in: K.A. Gscheidner Jr., L. Eyring (Eds.), Handbook on the Physics and Chemistry of Rare Earths, North-Holland, Amsterdam, 1979, p. 192ff.